Available online at www.sciencedirect.com
ScienceDirect
Journal of Power Sources 169 (2007) 276–287
JOURNAL OF POWER SOURCES
www.elsevier.com/locate/jpowsour

Study of pulsed-current loading of direct methanol fuel cells using a new time-domain model based on bi-functional methanol oxidation kinetics

Eric Vilar*, R.A. Dougal

Department of Electrical Engineering, University of South Carolina, Columbia, SC 29208, United States

Received 24 January 2007; received in revised form 12 March 2007; accepted 12 March 2007
Available online 15 March 2007

Abstract

This work describes a non-linear time-domain model of a direct methanol fuel cell (DMFC) and uses that model to show that pulsed-current loading of a direct methanol fuel cell does not improve average efficiency. Unlike previous system level models, the one presented here is capable of predicting the step response of the fuel cell over its entire voltage range. This improved model is based on bi-functional methanol oxidation reaction kinetics and is derived from a lumped, four-step reaction mechanism. In total, six states are incorporated into the model: three states for intermediate surface adsorbates on the anode electrode, two states for the anode and cathode potentials, and one state for the liquid methanol concentration in the anode compartment. Model parameters were identified using experimental data from a real DMFC. The model was applied to study the steady-state and transient performance of a DMFC with the objective to understand the possibility of improving the efficiency of the DMFC by using periodic current pulses to drive adsorbed CO from the anode catalyst. Our results indicate that the pulsed-current method does indeed boost the average potential of the DMFC by 40 mV; but on the other hand, executing that strategy reduces the overall operating efficiency and does not yield any net benefit.
Published by Elsevier B.V.

Keywords: Direct methanol fuel cell; Dynamic simulation; Transient response; Modeling; Pulse loading

1. Introduction

Several studies of the transient voltage response of direct methanol fuel cells (DMFCs) have been reported. Carrette et al. discussed a pulsed-current loading method that seemingly cleansed the anode catalyst of accumulated CO, resulting in a voltage response that rose to a peak value as CO adsorbate was oxidized from the anode catalyst and then slowly relaxed to a steady-state value as the CO again filled catalyst sites [1]. Carrette experimented with a PEM fuel cell fed with hydrogen gas containing CO, but others have reported the same sort of transient responses for gas-fed [2] and liquid-fed DMFCs [3,4]. Argyropoulos et al. observed that their fuel cell overshot the open-circuit potential by more than 100 mV whenever the load current was suddenly reduced to zero [3], and later observations by Yoo et al. showed that variations in the size and duration of the overshoot depend on the size of the current step [5]. In addition, to discussing the cleansing dynamic occurring at the anode electrode, some of these researchers have speculated that methanol crossover also impacts the transient response of liquid-fed DMFCs by varying the mixed potential reaction at the cathode catalyst. However, in a more recent study, Neergat et al. measured the anode potential against a dynamic hydrogen electrode during a pulsed-current sequence and they found that most of the voltage transient measured at the terminal of the fuel cell is due to the response of the anode overpotential [6].

State-of-the-art DMFCs oxidize methanol through a bi-functional mechanism that enhances the oxidation rate of CO at lower anode potentials by using catalysts containing a combination of platinum and ruthenium [7]. It is generally accepted that methanol and hydroxyl adsorption occur independently on separate reaction sites, but no firm consensus has been reached on the reaction mechanics. As a result, several variations of mathematical models describing the process are reported in the literature. For instance, Divisek et al. accounted for eight reaction steps, including a four-step methanol dehydrogenation process and dual parallel pathways for CO oxidation [8], whereas other researchers have been equally successful by simply presuming

* Corresponding author. Tel.: +1 803 777 7890; fax: +1 803 777 8045.
E-mail address: vilar@engr.sc.edu (E. Vilar).

0378-7753/$ – see front matter. Published by Elsevier B.V.
doi:10.1016/j.jpowsour.2007.03.024

Nomenclature

A	weight for individual steady-state data points
B	weight for individual transient data points
c	methanol concentration (mol cm^{-3})
C	electrical capacitance (F cm^{-2})
d	duty ratio
D	methanol diffusivity in water (cm^2 s^{-1})
E_{SS}	error for an entire steady-state curve
E_{TR}	error for an entire transient response
E_{total}	total combined error to be minimized
F	Faraday constant (96,485 A s)
ΔG	Gibbs free energy (J mol^{-1})
i	charge transfer rate (A cm^{-2})
i_{load}	external load current (A cm^{-2})
i_{leak}	internal leakage current (A cm^{-2})
i_p	parasitic current due to methanol crossover (A cm^{-2})
I_{load}	average external load current (A cm^{-2})
k	reaction rate coefficient (mol s^{-1} cm^{-2})
K	mass transfer coefficient (cm s^{-1})
L	thickness (cm)
p	oxygen pressure (bar)
P_a	average power dissipated in the anode reaction (W cm^{-2})
P_{load}	average power transferred to the external load (W cm^{-2})
r	reaction rate (mol s^{-1} cm^{-2})
R	gas constant (8.314 J K^{-1} mol^{-1})
T	temperature (K)
ΔT	time period of load cycle (s)
u	electrical potential (V)
u_{load}	external load voltage (V)
U_o	ideal open-circuit potential (1.21 V)
U_{load}	average external load voltage (V)
V	characteristic length (cm)
W_A	weight for one entire steady-state curve
W_B	weight for one entire transient response

Greek symbols

Γ	mole density (mol cm^{-2})
α	transfer coefficient
ε	porosity
η	constant-load steady-state efficiency
η_T	periodic-load steady-state efficiency
θ	fractional surface coverage
σ_{leak}	leakage conductance (S cm^{-2})
σ_{PEM}	membrane conductance (S cm^{-2})
τ	tortuosity or time constant (s)

Subscripts

0	at standard conditions
a	anode
c	cathode
f	external supply
PEM	membrane
pt	platinum region
ru	ruthenium region

a one-step dehydrogenation process and a single pathway for CO oxidation [9–12]. In general, the reaction mechanism can be described in several condensed variations, with each model depending on the system context.

The models described above were defined only for steady-state conditions; system-level models of DMFCs that apply under transient conditions have been scarce. Sundamacher et al. developed a model to explain the voltage response to step variations in the concentrations of methanol fed to the fuel cell. In order to eliminate the transient adsorption/desorption dynamics of the oxidation reaction, they assumed that the intermediate reaction steps were in equilibrium. Also, they did not analyze the voltage response to step changes in current [13]. In a later study, Krewer and Sundmacher replaced the bi-functional oxidation kinetics of the earlier model with a concise two-step reaction that added a state for adsorbed CO. They used experimental step-response measurements to identify the parameter values for a linearized version of their model, but the linearized model predicted a peak voltage overshoot that was only one-tenth of the experimental value [14]. In this work, we go beyond previous system-level models by applying the bi-functional reaction mechanism to develop a mathematical model of the DMFC that has sufficient detail to predict the transient response of the fuel cell voltage caused by large step changes of current under no-load and full-load conditions.

2. Theory

2.1. Model description

The methanol oxidation reaction can be differentiated into two sequential steps. First, the methanol is dehydrogenated in a process that produces stable CO adsorbates on the surface of the electrode; then, the adsorbates are oxidized to CO_2 and thereby freed from the surface [7]. On platinum-ruthenium catalysts, the reaction proceeds through a bi-functional mechanism where the platinum regions adsorb and dehydrogenate methanol, and the ruthenium regions dissociate H_2O into OH groups. The resulting CO and OH adsorbates then react at the boundaries of the two metals where the intermediates collide.

The entire electrochemical process can be more formally described by the following reaction mechanism:

$$CH_3OH \leftrightarrow Pt\text{–}CH_2OH + H_{ads} \quad (1)$$

$$Pt\text{–}CH_2OH \leftrightarrow Pt_2\text{–}CHOH + H_{ads} \quad (2)$$

$$Pt_2\text{–}CHOH \leftrightarrow Pt_3\text{–}COH + H_{ads} \quad (3)$$

$$Pt_3\text{–}COH \leftrightarrow CO_{ads} + H_{ads} \quad (4)$$

$$H_{ads} \leftrightarrow H^+ + e^- \quad (5)$$

$$H_2O \leftrightarrow OH_{ads} + H^+ + e^- \quad (6)$$

$$CO_{ads} + OH_{ads} \leftrightarrow CO_2 + H^+ + e^- \quad (7)$$

Reaction steps (1)–(4), discussed in refs. [7] and [9], describe the dehydrogenation process of methanol (CH_3OH) on platinum, in which hydrogen is stripped from methanol in successive steps until a final stable intermediate of CO_{ads} is formed. Step (5) is the hydrogen desorption from the catalyst surface, which according to refs. [9] and [15] is slow at low potentials. The two remaining steps describe the extraction of OH_{ads} from water on ruthenium and the subsequent oxidative removal of CO_{ads} from the surface of the catalyst; these steps account for only a single pathway for CO_{ads} oxidation, as in ref. [11].

The time-domain model defined here is simplified by lumping all of the reactions defined in (1)–(4) into a single step as shown in (8).

$$CH_3OH \leftrightarrow CO_{ads} + 4H_{ads} \quad (8)$$

This also conveniently reduces the number of otherwise unknown kinetic parameters. However, as a tradeoff, CO_{ads} and H_{ads} become ambiguous quantities that encompass intermediates from the eliminated steps.

The set of rate equations for this lumped reaction mechanism is defined as follows by assuming Langmuir conditions:

$$r_1 = k_1 \left(\frac{c_a}{c_o}\right)(1 - \theta_{CO} - \theta_H) \quad (9)$$

$$r_2 = k_2\theta_H e^{u_a\alpha_2 F/RT} - k_2'(1 - \theta_{CO} - \theta_H) e^{u_a(\alpha_2 - 1)F/RT} \quad (10)$$

$$r_3 = k_3(1 - \theta_{OH}) e^{u_a\alpha_2 F/RT} - k_3'\theta_{OH} e^{u_a(\alpha_3 - 1)F/RT} \quad (11)$$

$$r_4 = k_4\theta_{CO}\theta_{OH} e^{u_a\alpha_4 F/RT} \quad (12)$$

We describe the adsorption of methanol without charge transfer, and so its reaction rate, r_1, is expressed without potential dependence, whereas the remaining three reactions for hydrogen desorption, r_2, water dissociation, r_3, and CO oxidation, r_4, are potential-dependent. We further apply the following conventional assumptions: the methanol adsorption reaction is first order, the activity of water is unity and the charge transfer coefficients are symmetrical. The rate expressions above are given in mol cm^{-2} s^{-1}, and so the total charge transfer rate in A cm^{-2} is related through the Faraday constant in (13).

$$i_a = F(r_2 + r_3 + r_4) \quad (13)$$

For simplicity, we take the reference concentration to be unity, $c_0 = 1$ mol L^{-1}, and omit it in the remainder of this document.

The anode electrode is modeled with a total of five state variables: one state for the fractional coverage of each of the three adsorbates on the anode catalyst, θ_{CO}, θ_H and θ_{OH}, plus states for the anode overpotential, u_a, and the methanol concentration in the active layer of the anode compartment, c_a. The dynamic system is coupled by the following set of state equations.

$$\Gamma_{Pt}\frac{d\theta_H}{dt} = 4r_1 - r_2 \quad (14)$$

$$\Gamma_{Pt}\frac{d\theta_{CO}}{dt} = r_1 - r_4 \quad (15)$$

$$\Gamma_{Ru}\frac{d\theta_{OH}}{dt} = r_3 - r_4 \quad (16)$$

$$C_a\frac{du_a}{dt} = i_{load} + u_{load}\sigma_{leak} - F(r_2 + r_3 + r_4) \quad (17)$$

$$V_a\frac{dc_a}{dt} = K_a(c_f - c_a) - K_{PEM}c_a - r_1 \quad (18)$$

Eqs. (14)–(16) express mole balances for the adsorbates bonded to the surface of the catalyst; (17) describes the charge balance at the anode double layer, including a term for the leakage-current ($i_{leak} = u_{load}\sigma_{leak}$); and (18) defines the mole balance for methanol in the anode compartment. The last state equation applies to the active region of the electrode and balances the influx of methanol, its reaction rate at the catalyst, and the outflux due to methanol crossover.

Methanol crossover describes the process of methanol diffusing past the anode catalyst layer through small pores in the polymer electrolyte membrane (PEM) to the cathode, where it can directly combine with oxygen at the cathode catalyst. This represents a parasitic side-reaction that increases polarization losses and reduces the efficiency of the fuel cell. According to Dohle et al., experiments show that 80–100% of the methanol reaching the cathode can react there depending on the operating conditions [16]. In our model, we follow the simplified approach of Sundmacher et al. in ref. [13] and presume that all of the methanol that reaches the cathode reacts instantaneously. Hence, the parasitic reaction rate is limited only by the flux of methanol through the PEM. The side reaction causes an equivalent parasitic current load on the cathode electrode, and that current is proportional to the crossover flux,

$$i_p = 6F(K_{PEM}c_a) \quad (19)$$

in which six electrons are transferred per mole of methanol consumed in the side reaction.

This parasitic current is coupled with the system dynamics through the charge balance at the cathode electrode.

$$C_c\frac{du_c}{dt} = i_{load} + u_{load}\sigma_{leak} + 6F(K_{PEM}c_a) - i_c \quad (20)$$

Here, u_c is the cathode polarization loss and i_c is the charge transfer rate of the normal oxygen reduction reaction. Unlike the complex mechanics applied to anode reactions, the oxygen reduction reaction is taken to occur in a single rate-determining step, and the reaction rate is described by Tafel kinetics as:

$$i_c = 6Fk_5(p_c/p_0) e^{u\alpha_5 F/RT} \quad (21)$$

where $p_0 = 1.0$ bar.

Polarization losses at the anode and cathode electrodes are asymmetric. In the cathode, polarization losses are caused by a combination of externally applied electrical loads and methanol crossover, which fuels the parasitic side reaction. The parasitic reaction rate is fastest under no-load conditions when the concentration in the active region is greatest, and the rate slows when an external load is applied because the concentration in

the active region decreases somewhat. Thus, the cathode is effectively under a sustained current regardless of the external load, because the parasitic current subsides as the external current load increases. On the other hand, methanol crossover does not impact the anode electrode, and so the anode polarization loss is due primarily to the external load. Moreover, because of the combined impact of slow methanol oxidation kinetics and transfer losses of liquid methanol to the active region, the overpotential at the anode dominates the overall voltage–current dynamics of the fuel cell. For the purposes of this study, the anode is modeled over its entire potential range, whereas the asymmetry between the electrodes allows the cathode to be modeled only within the active region, such that concentration overpotentials due to oxygen transfer are negligible.

2.2. Calculating efficiency

The output voltage of the fuel cell is reduced by anodic and cathodic polarization losses plus some ohmic loss that is significant at higher currents due to the limited proton conductance of the PEM. The load voltage is described by:

$$u_{\text{load}} = u_{\text{o}} - u_{\text{a}} - u_{\text{c}} - \sigma_{\text{PEM}}^{-1} i_{\text{load}} \tag{22}$$

The first right-hand term in (22), u_{o}, is the ideal open-circuit potential of a DMFC. It is directly related to the maximum energy that can be converted from the methanol fuel, and its value is determined by the Gibbs free energy of the methanol combustion reaction.

$$u_{\text{o}} = \frac{\Delta G}{6F} \tag{23}$$

This maximum potential term is also useful for calculating the efficiency of a fuel cell from its electrical dynamics as discussed in ref. [16]. Under a constant load, the efficiency is given by the following power ratio:

$$\eta = \frac{u_{\text{load}} i_{\text{load}}}{u_{\text{o}}(i_{\text{load}} + i_{\text{p}} + i_{\text{leak}})} \tag{24}$$

where the numerator is the electrical power delivered to the externally connected load, and the denominator is the total power released by the chemical reaction. Under pulsed-loading regimes, which have been proposed to improve the performance of a DMFC, the fuel cell achieves a periodic steady-state during which CO_{ads} is cleansed from the anode surface at regular intervals. Under these schemes, the efficiency is measured by integrating the numerator and denominator of (24) over the interval of one pulse cycle.

$$\eta_{\text{T}} = \frac{1}{u_{\text{o}}} \frac{\int_{\Delta T} (u_{\text{load}} i_{\text{load}}) \text{d}t}{\int_{\Delta T} (i_{\text{load}} + i_{\text{p}} + i_{\text{leak}}) \text{d}t} \tag{25}$$

Hence, the different loading schemes can be compared using this model by measuring the efficiency of the fuel cell under equivalent constant-current and pulsed-current loads. Table 1 lists additional calculations (26)–(29) that are useful for analyzing the average performance of the DMFC at periodic steady state.

Table 1
Average value calculations

Definition	Expression	
Average load current (A cm^{-2})	$I_{\text{load}} = \Delta T^{-1} \int_{\Delta T} i_{\text{load}} \, \text{d}t$	(26)
Average load voltage (V)	$U_{\text{load}} = \Delta T^{-1} \int_{\Delta T} u_{\text{load}} \, \text{d}t$	(27)
Average load power (W cm^{-2})	$P_{\text{load}} = \Delta T^{-1} \int_{\Delta T} u_{\text{load}} i_{\text{load}} \, \text{d}t$	(28)
Average power dissipated in the anode reaction (W cm^{-2})	$P_{\text{a}} = \Delta T^{-1} \int_{\Delta T} u_{\text{a}} (i_{\text{load}} + i_{\text{leak}}) \text{d}t$	(29)

2.3. Parameter identification

The performance of the DMFC can be generalized by four processes that influence the voltage–current characteristic of the fuel cell. We identify these processes in Fig. 1 with their regions of influence mapped on the *V–I* plane. In the first region, mixed-potential losses at the cathode electrode due to parasitic and applied current loads dominate; the combined losses are approximately constant over the entire current range of the fuel cell. In the second region, the no-load activation losses at the anode electrode dominate. We presume these to be about equal to the amount of voltage overshoot observed when the current load is suddenly removed from the DMFC. In the third and fourth regions, activation losses increase with current due to a combination of CO oxidation and proton conductance through the PEM. In the fourth region, polarization losses increase more rapidly due to the limited rate at which methanol can diffuse to the anode region and be adsorbed onto the anode catalyst.

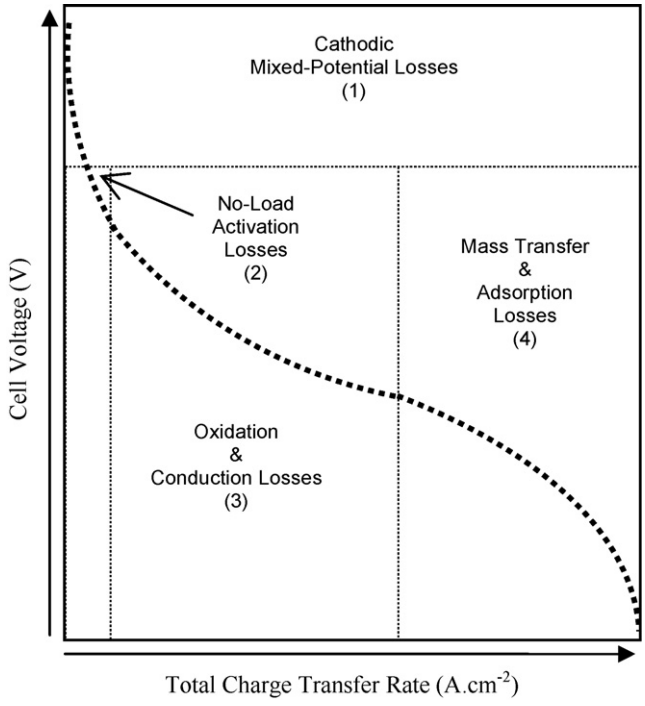

Fig. 1. Typical voltage–current characteristic of a DMFC showing regions that correspond to dominant processes affecting the polarization of the fuel cell.

Because half-cell measurements have not been published for the DMFC analyzed in this work, the anode overpotential at steady-state is estimated from experimental data using the following:

$$u_a \approx u_o - u_c(i_{load}) - u_{load}(i_{load}) - \sigma_{PEM}^{-1} i_{load} \tag{30}$$

in which i_{load} is the load current drawn from the fuel cell, u_{load} the measured output voltage as a function of i_{load}, and u_c is the calculated polarization loss at the cathode electrode also as a function of i_{load}. In the analysis here, the cathode potential is initially presumed constant and equal to its open-circuit value so that the parameters describing the dynamics in ranges 2–4 of Fig. 1 can be independently identified. We estimate the cathode potential from experimental data using:

$$u_c(0) \approx u_o - u_{load}(0) - u_a(0) \tag{31}$$

in which the no-load anode potential is estimated on the basis of the observed voltage overshoot of the DMFC. After the model parameters for the decoupled system are initially identified, the cathode dynamics are introduced to the model, and the reaction rate coefficient, k_5, is calculated from (21) under the no-load condition with known values for u_c, a_5, c_c and K_{PEM}. The last parameter, K_{PEM}, is calculated based on the material properties of the membrane according to:

$$K_{PEM} = \varepsilon^{\tau} \frac{D_{CH_3OH}}{L_{PEM}} \tag{32}$$

An analytical expression for the steady-state load current cannot be easily derived from the state-space system described in (14)–(18) and (20), and so we alternatively solve the system by (a) recognizing that the steady-state current can be expressed as $i_a = 6Fr_4$, (b) combining only (14)–(16) to obtain an analytical expression for the current as a function of the anode overpotential and of the methanol concentration, and (c) implicitly solving for the concentration of methanol in the anode compartment. However, even with these simplifications, the expression is too cumbersome to be useful for much more than computational analysis and it is not presented here.

On the other hand, some analysis is possible without eliminating every dependent variable. In particular, the anode current can be expressed at steady-state as a function of θ_{OH} and u_a.

$$i_a = \frac{6Fk_1k_2k_4c_a\theta_{OH}}{k_2k_4\theta_{OH} + k_4k_2'\theta_{OH}\,e^{-u_aF/RT} + 4k_1k_4c_a\theta_{OH}\,e^{-u_a\alpha_2F/RT} + k_1k_2c_a\,e^{-u_a\alpha_4F/RT}} \tag{33}$$

By evaluating this expression at the upper voltage limit, the maximum load current is found to be:

$$i_a \le 6Fk_1c_a \tag{34}$$

Partial solutions for the steady-state surface coverage terms can be expressed in the same manner.

$$\theta_H = \frac{(4k_1c_a + k_2'\,e^{u_a(\alpha_2-1)F/RT})(1-\theta_{CO})}{4k_1c_a + k_2\,e^{u_a\alpha_2F/RT} + k_2'\,e^{u_a(\alpha_2-1)F/RT}} \tag{35}$$

$$\theta_{CO} = \frac{k_1c_a(1-\theta_H)}{k_1c_a + k_4\theta_{OH}\,e^{u_a\alpha_4F/RT}} \tag{36}$$

$$\theta_{OH} = \frac{k_3}{k_3 + k_3'c_a\,e^{-u_aF/RT} + k_4\theta_{CO}\,e^{u_a(\alpha_4-\alpha_3)F/RT}} \tag{37}$$

The expression for θ_{OH} reveals that the coverage of OH_{ads} on ruthenium approaches zero at no-load if $k_3 \ll k_3' + k_4$, and the OH_{ads} coverage approaches unity at high potentials if $\alpha_3 > \alpha_4$. The expressions for θ_{CO} and θ_H do not provide additional insight about model parameters; however, the equations do indicate that the surface coverages of H_{ads} and CO_{ads} approach zero at the high voltage limit.

Many of the parameters are fitted using a searching algorithm that attempts to minimize the error between modeled and experimental data. In particular, we apply a modified version of the standard *fminsearch* function in MATLAB, *fminsearchbnd*, which is available from the Mathworks website. The total error is composed of two data sets: one to compare steady-state values and another to compare the transient responses. These functions are defined as follows:

$$E_{SS} = \sum_i A_i[i_{load,ex}(u_a|_i) - i_{load,th}(u_a|_i)]^2 \tag{38}$$

$$E_{TR} = \sum_j B_j[u_{load,ex}(t|_j) - u_{load,th}(t|_j)]^2 \tag{39}$$

The steady-state errors are evaluated for load currents at discrete values of the anode overpotential, whereas the transient errors are evaluated for the load voltage at discrete instances of time.

The two errors are combined into a larger function so that they can be minimized simultaneously.

$$E_{Total} = \sum_k W_{A,k}E_{SS,k} + \sum_m W_{B,m}E_{TR,m} \tag{40}$$

In practice, the algorithm must be repeated many times to identify the model, and between each repetition, it is often necessary to manually adjust some weights and parameters to improve poorly fit regions of data. Results of the parameter identification will be described next.

3. Results and discussion

3.1. Parameter identification

The purpose of this research is to model the transient response of the DMFC voltage to step changes in the load current. To achieve that, we apply the bi-functional multi-step methanol oxidation mechanism to describe the transient voltage response of the DMFC anode, and we also apply some methanol crossover dynamics to account for transient losses at the cathode. The model description does not go so far as to incorporate higher-level effects related to stack temperature, air humidity and stoichiometric flow rates, making its application limited in scope. These other operating conditions are controllable at the system level, and it is necessary to regulate them to near constant values if the parameters for this model are to be properly identified.

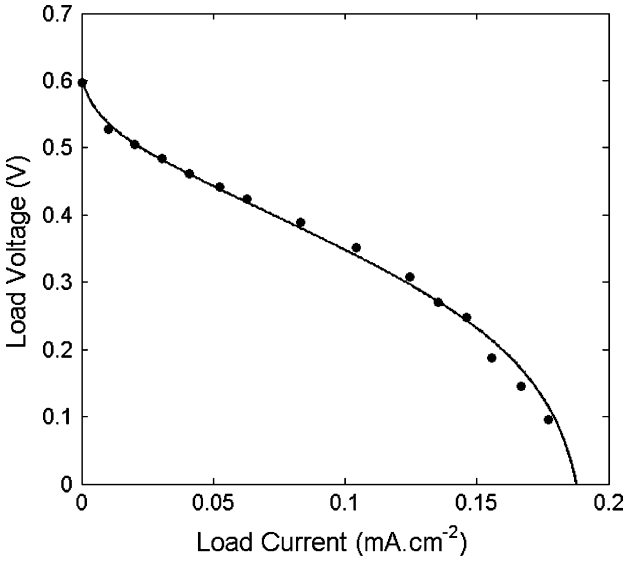

Fig. 2. Steady-state polarization curves from the model (solid line) and from the experiment (data points).

Krewer and Sundmacher developed a DMFC mini-plant with pre-heaters that regulate the air and methanol fuel temperatures and large pumps that supply very high flow rates of air and methanol to the fuel cell [14]. Due to the pre-heating and high flow rates, the stack temperature and fuel properties are effectively constant regardless of the electrical load condition; therefore, the data reported for this DMFC are particularly well suited for parameterizing the model in this work. Their DMFC consists of a single 26 cm^2 cell with a Nafion 105 membrane.

The four sets of experimental data used to parameterize the model are plotted in Figs. 2 and 3 along with the corresponding simulated data from the parameterized model. In every case, the experimental DMFC is operated at 1.7 bar and 333 K and is supplied 1.0 mol L^{-1} of pre-heated methanol at 0.5 L min^{-1} and dry air at 8.333 slpm [14]. The first figure plots the load voltage measured at the terminals of the fuel cell, and the second figure plots the transient voltage waveforms for three different step-loading conditions. Two of the step loads result in a long transient response. The voltage response to current step-down from full load (0.157 A cm^{-2}) to no-load (0 A cm^{-2}) requires about 220 s to settle whereas the voltage response to current step-up from partial load (0.026 A cm^{-2}) to full load (0.157 A cm^{-2}) requires about 160 s to complete. Finally, the response to a current step down that lies within the normal operating range of the fuel cell (from 0.052 down to 0.026 A cm^{-2}) is comparatively fast, requiring only about 20 s to reach steady state.

Due to an unexplained influence affecting voltage measurements, the voltage among the four data sets varies by a maximum of about 25 mV at steady state, making it difficult to parameterize the model equally well for each case. Before calculating the error, E_{TR}, in (39), we handle the measurement inconsistency by normalizing the transient data using the following method:

$$\hat{u}_{load} = \frac{u_{load}(t) - u_{load}(t_0)}{u_{load}(t_f) - u_{load}(t_0)} \tag{41}$$

In this way, the error is calculated relative to the change in the load without influence from the initial and final values of the load voltage. The polarization data in Fig. 2 are not normalized before calculating the error, E_{SS}, so the polarization data are the only steady-state reference for parameterizing the DMFC model.

Table 2 lists the parameters for the DMFC model; it indicates which parameters are fitted, which parameters are known values,

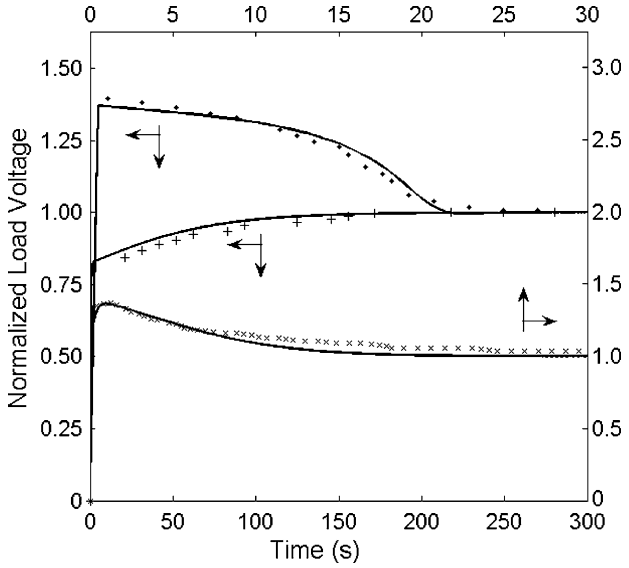

Fig. 3. Transient voltage responses for three different load changes: the extreme current step-down response from full load (0.157 A cm^{-2}) to no-load (0 A cm^{-2}) (♦), the current step-up response from partial load (0.026 A cm^{-2}) to full load (0.157 A cm^{-2}) (+) and the moderate step-down response from 0.052 to 0.026 A cm^{-2} (×). Solid lines are model data. Load voltages are normalized to permit comparison between model and experiment.

Table 2
Model parameters

Symbol	Value	Method
C_a	13.3×10^{-3} F cm^{-2}	Fit
C_c	41.7×10^{-3} F cm^{-2}	[20]
D	38.1×10^{-6} cm^2 s^{-1}	[17]
k_1	67.3×10^{-6} mol s^{-1} cm^{-2}	Fit
k_2	80.5×10^{-9} mol s^{-1} cm^{-2}	Fit
k_2'	49.7×10^{-8} mol s^{-1} cm^{-2}	Fit
k_3	17.1×10^{-10} mol s^{-1} cm^{-2}	Fit
k_3'	17.8×10^{-12} mol s^{-1} cm^{-2}	Fit
k_4	20.5×10^{-9} mol s^{-1} cm^{-2}	Fit
k_5	42.3×10^{-15} mol s^{-1} cm^{-2}	Calculated
K_a	1.0×10^{-3} cm s^{-1}	Fit
L_{PEM}	12.7×10^{-3} cm	[14]
V_a	53.6×10^{-3} cm	Calculated
a_2	0.320	Fit
a_3	0.830	Fit
a_4	0.265	Fit
a_5	0.875	[17]
Γ_{pt}	5.51×10^{-7} mol cm^{-2}	Fit
Γ_{ru}	7.99×10^{-7} mol cm^{-2}	Fit
ε	0.3	[17]
σ_{leak}	3.74×10^{-3} S cm^{-2}	Fit
σ_{PEM}	7.69 S cm^{-2}	[21]
τ	1.8	[17]

and which parameters are calculated. The material properties for N105 membranes in liquid DMFCs have not been well reported in the literature, and so it was necessary to take parameters for the PEM porosity and tortuosity from a similar membrane. In this analysis, these parameters are taken from ref. [17] for an N112 membrane. In comparison to the N105 PEM used in the experimental study, the equivalent weight of the N112 PEM is 10% larger.

The remaining unknown parameters are identified or calculated by the process summarized in Section 2.3 with two exceptions. The material properties for the anode compartment, K_a and V_a, are identified using the full-load step response of the DMFC, which slowly drops by 50 mV as the result of methanol slowly decreasing in the anode compartment. We presume that the time derivatives of methanol concentration and voltage are proportional after the initial 200 mV drop such that the following is true:

$$\lambda(\mathrm{d}c_a) = \mathrm{d}u_{load} = u_{load}(t_f) - (u_{load}(t_0) - u_{load}(t_f))\,\mathrm{e}^{-t/\tau} \quad (42)$$

The characteristic length of the anode compartment, V_a, is then related to the mass transfer coefficient as follows:

$$V_a = \tau(K_a + K_{PEM}) \quad (43)$$

where τ is the time constant in (42) and is calculated from the experimental data. The value of K_a is determined by incrementally increasing its value until the full-load step response has a voltage at t_0 that is approximately 80% of the final value.

3.2. Steady-state characteristics

The predicted steady-state polarization curves for the fuel cell when the methanol feed concentration ranges from 0.25 to 2.0 mol L^{-1} are plotted in Fig. 4 with the reference case $c_f = 1.0$ mol L^{-1} drawn with a bold line. The predicted polarization curves are typical and are consistent with results reported throughout the literature. When the load current is small, the polarization curves are tightly grouped, but as the current increases, the voltages diverge toward zero in succession, beginning with the curve with the lowest methanol concentration. This figure also shows the effect of the load current on the internal concentration of methanol in the anode compartment. Under a no-load condition, the concentration in the anode is somewhat less than the concentration supplied to the fuel cell because some methanol diffuses past the anode catalyst through the PEM. At maximum current, the concentration is only reduced to about 50%, indicating that the predominant factor limiting the current is methanol adsorption onto the catalyst and not methanol transfer through the backing layer of the fuel cell.

Increasing the methanol feed concentration boosts the load capacity of the fuel cell, but at the cost of also increasing the rate of methanol crossover, thereby making the fuel cell less efficient. This trade-off is demonstrated in Fig. 5: when supplied 0.25 mol L^{-1} methanol concentration the efficiency of the DMFC peaks at 20% and the no-load parasitic current is 37 mA cm^{-2}, but when the concentration is increased to 1.0 mol L^{-1}, the peak efficiency drops to 13% and the no-load parasitic current rises to 150 mA cm^{-2}. This model predicts poor efficiencies for this fuel cell, which can be explained in part by the nominal 60 °C operating temperature, which causes high activation losses, and the thin N105 membrane, which allows high rates of methanol crossover (a standard N117 membrane is 40% thicker). Perhaps the largest factor contributing to poor efficiency is the limited load capacity of this fuel cell, which has a maximum current of only 185 mA cm^{-2} at the reference concentration. In contrast, Neergat et al. achieved current densities of 450 mA cm^{-2} with their DMFC using the same methanol concentration and operating temperature [6].

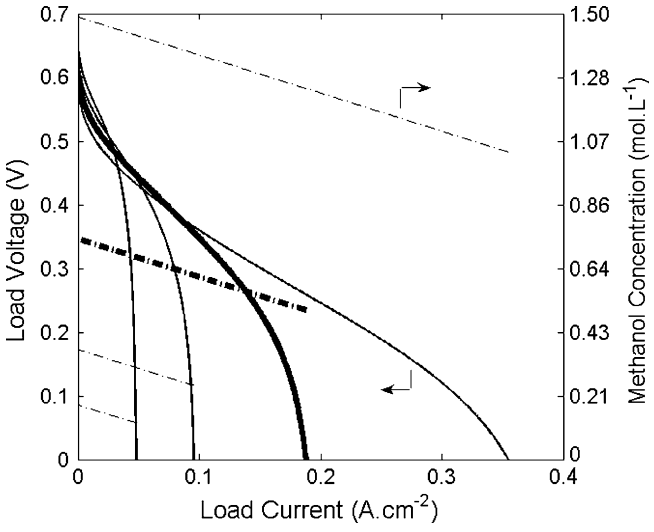

Fig. 4. Terminal voltage of the fuel cell available to the load (left axis) and the methanol concentration in the anode compartment (right axis), as functions of load current and methanol feed concentration. The feed concentrations are 0.25, 0.5, 1.0 and 2.0 mol L^{-1}, and the bolded lines correspond to $c_f = 1.0$ mol L^{-1}.

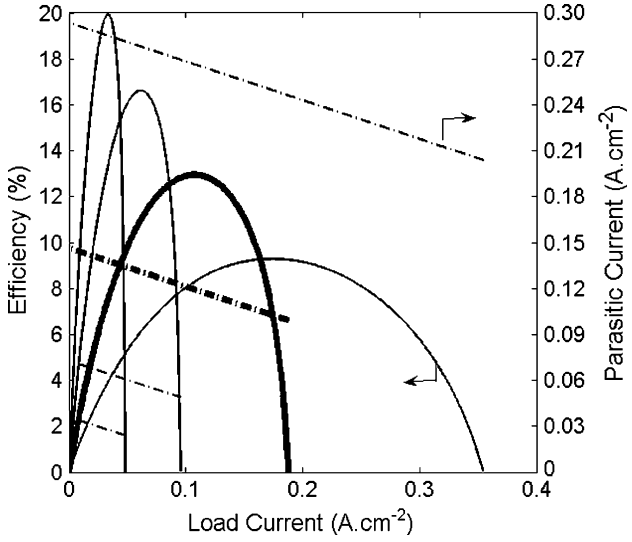

Fig. 5. Efficiency of the DMFC (left axis) and the parasitic current (right axis), as functions of load current and methanol feed concentration. The feed concentrations are 0.25, 0.5, 1.0 and 2.0 mol L^{-1}, and the bolded lines correspond to $c_f = 1.0$ mol L^{-1}.

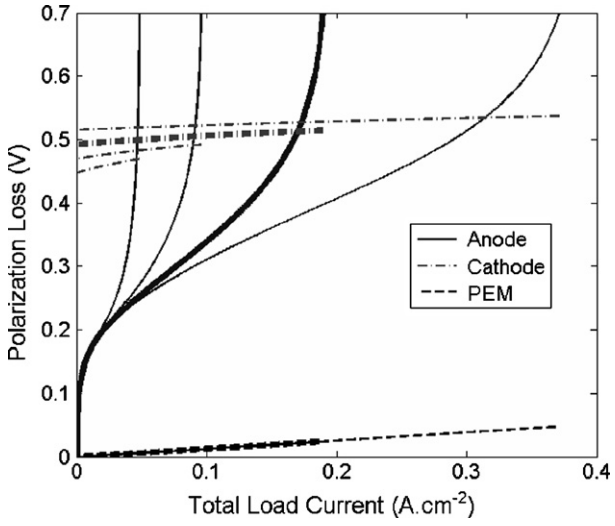

Fig. 6. Potential losses in steady state at each electrode and across the membrane as functions of load current and methanol feed concentration. The feed concentrations are 0.25, 0.5, 1.0 and 2.0 mol L^{-1}, and the bolded lines correspond to $c_f = 1.0$ mol L^{-1}.

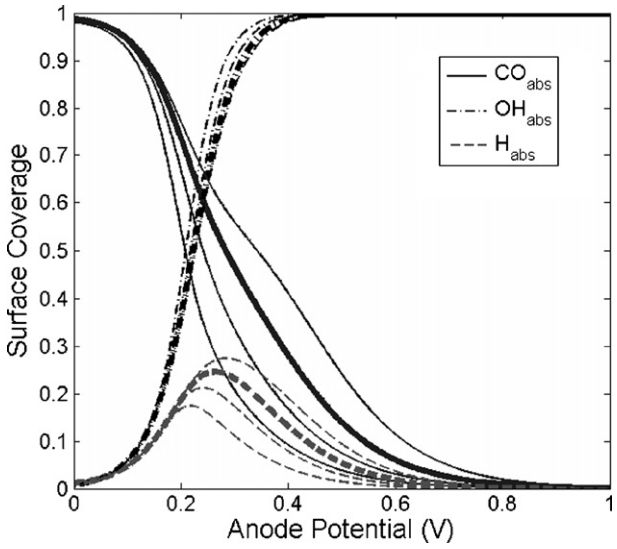

Fig. 7. Fractional surface coverages of adsorbed intermediates (θ_{CO}, θ_{OH} and θ_H) on the anode in steady state as functions of load current and methanol feed concentration. The feed concentrations are 0.25, 0.5, 1.0 and 2.0 mol L^{-1}, and the bolded lines correspond to $c_f = 1.0$ mol L^{-1}.

The polarization curves of the anode and cathode electrodes are plotted in Fig. 6 as functions of the total load current, which is defined as the summation of the load and leakage currents: i_{load} plus i_{leak}. Unlike the anode potential, the cathode is polarized by the parasitic side reaction because of methanol crossover. The zero-current potential at the cathode has a typical value of 475 mV and fluctuates by ±35 mV, depending on the methanol concentration in the fuel supply. The anode activation loss is steep at low currents, rising from 0 to 200 mV with just a small 20 mA cm^{-2} load. Due to the leakage current that causes some activation loss in the anode, the actual no-load polarization loss at the anode is 120 mV, which is within the peak overshoot observed at the no-load condition but 30–130 mV less than the no-load half-cell potentials measured in refs. [6,18,19].

Fig. 7 shows the surface coverages of the three intermediates on the anode catalyst as functions of the anode overpotential in steady state. At no-load, CO_{ads} covers nearly all platinum catalyst sites because little OH_{ads} is available to facilitate the oxidation of CO_{ads}. However, as the load increases, more OH_{ads} accumulates on the ruthenium surface and the oxidation rate improves. The higher oxidation rate purges CO_{ads} from catalyst sites, and the newly cleared sites are subsequently filled with chemisorbed hydrogen. The hydrogen coverage crests at about 250 mV, signifying a transition in the rate-determining step from hydrogen desorption to methanol chemisorption at this potential. The anode potential and methanol concentration both affect the amount of CO_{ads} coverage at the anode. At 300 mV, the coverage ranges from 55% at 2.0 mol L^{-1} down to 20% at 0.25 mol L^{-1}. The same span is achieved at 2.0 mol L^{-1} when the anode potential is increased from 300 to 500 mV.

3.3. Pulsed-current loading

This model incorporates six states that describe the transient performance of the DMFC: u_a, u_c, c_a, θ_{CO}, θ_H and θ_{OH}. All of these states except the cathode potential, u_c, directly affect the transient dynamics at the anode, whereas only u_c and the methanol concentration, c_a (which drives methanol crossover), directly affect the transient dynamics at the cathode. Figs. 8 and 9 show the transient responses of these states to a pulsed-current load, which alternates between zero and the successively higher values of 0.026, 0.052, 0.105 and 0.157 A cm^{-2}. The first figure plots the voltage states of the anode and cathode electrodes as well as the terminal voltage of the DMFC and the load current drawn from the fuel cell. Fig. 8 reveals that the decrease of load

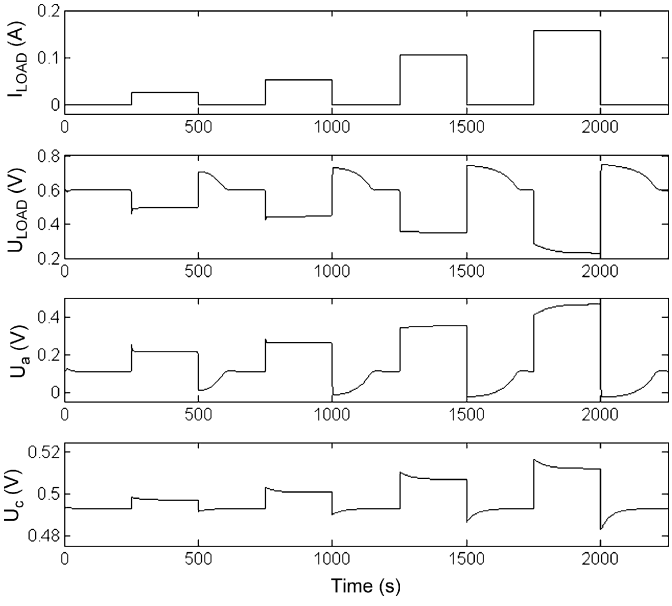

Fig. 8. Transient response of voltages to a pulsed-current load of increasing magnitude (current magnitude in succession for each pulse is 0.026, 0.052, 0.105 and 0.157 A cm^{-2}). Beginning with the topmost plot, the figure shows load current, load voltage, anode potential loss and cathode potential loss. The pulse period is 500 s.

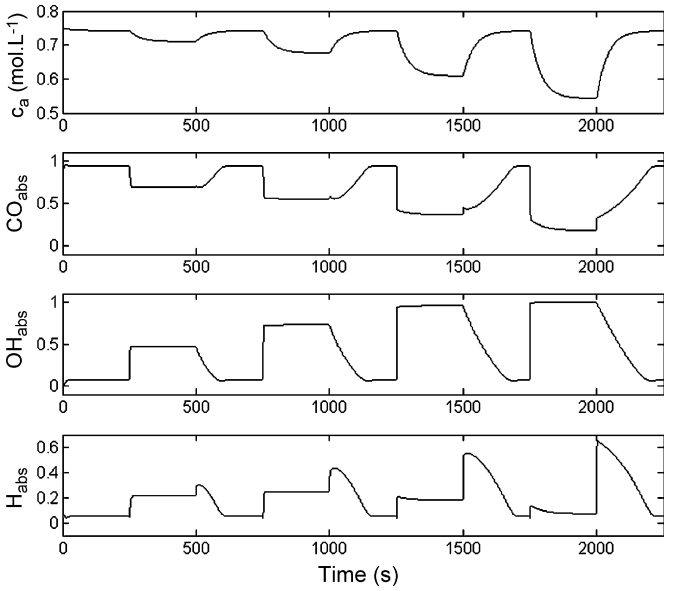

Fig. 9. Transient response of non-electrical states to a pulsed-current load of increasing magnitude (current magnitude in succession for each pulse is 0.026, 0.052, 0.105 and 0.157 A cm^{-2}). The topmost plot shows the methanol concentration in the anode compartment, and the remaining plots show in descending order the surface coverages θ_{CO}, θ_{OH} and θ_H. The pulse period is 500 s.

voltage is mainly attributed to anode losses which approaches 450 mV at full load, in contrast to cathode losses, which amount only to 30 mV at full load. Fig. 9 shows the methanol concentration in the anode compartment along with the coverages of the three adsorbates. From this figure, we note that the non-minimal phase response of θ_H significantly influences the overshoot and undershoot of the anode potential. A more detailed plot of these states is provided in Fig. 10. The non-minimum phase response of θ_H occurs because the first reaction step is taken to be voltage-independent in (9). Consequently, the deviation of r_1 lags behind the other reaction rates when the current load is interrupted, and so the reaction produces a temporary abundance or deficiency of hydrogen, depending on the direction of the current step. Interestingly, the peak overshoot of the anode potential diminishes with higher pulsed loads, such that eventually no voltage overshoot is discernable in the transient response when the DMFC is stepped up to a full-load condition. The same trend is observed in the experimental data of ref. [14], as well as for a different DMFC in refs. [3,4].

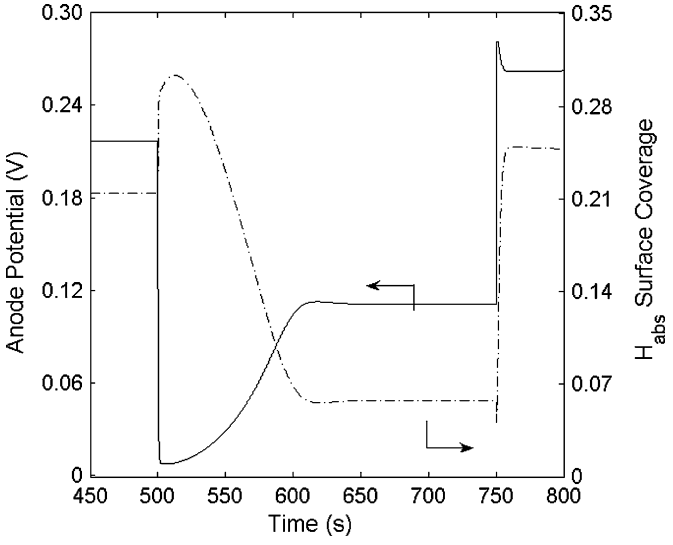

Fig. 10. Detailed view of the transient anode potential (left axis) and the transient surface coverage θ_H (right axis) from Figs. 8 and 9.

As outlined in Section 1, the literature reflects much interest regarding the possibility of cleansing CO_{ads} from the surface of the anode by intermittently increasing the current. It has been shown experimentally that these high current pulses temporarily raise the voltage available to the load, thereby creating a period of higher potential where a larger-than-normal amount of power might be delivered to the load. However, it has not been demonstrated that pulsed-current loading actually improves efficiency in comparison to a conventionally loaded DMFC supplying an equivalent constant current. Our next objective, then, was to investigate the efficiency of this process through simulation.

The simulation applies to the DMFC described in Section 3.1, in which the temperature and fuel supply rates are constant. Fig. 11 shows the voltage measured at the terminals of the fuel cell when it is nominally loaded at 0.026 A cm^{-2} and periodically pulsed to a full-load current of 0.157 A cm^{-2}. Several waveforms are plotted for pulse duties (ratio of pulse high time to pulse period) ranging from 0.5% to 20% in duration. In every case, the total pulse period is 20 s, and the waveforms are always plotted at periodic steady state. These results show that the peak voltage is a strong function of the duty ratio, with the largest voltage effect occurring when the duty ratio is large, and the minimum effect occurring when the duty ratio is small; however, the benefit appears to exhibit asymptotic behavior at both extremes of pulse duty. When the duty is large, a 100% increase of duty from 10% to 20% yields a negligible increase in the peak potential, and when the duty is small, a 100% increase from 0.5% to 1.0% also yields only a small increase in potential. Between

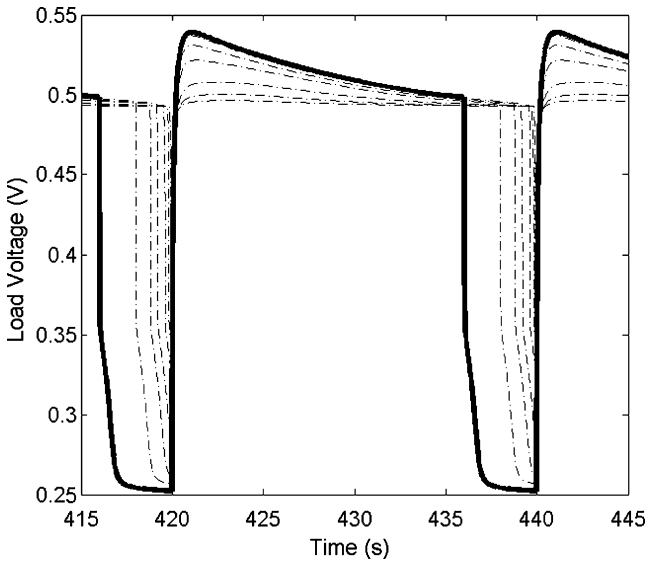

Fig. 11. Transient voltage responses at periodic steady state to pulse loads with the following duty ratios: 0.2 (solid line), 0.1, 0.06, 0.04, 0.02, 0.01 and 0.005. In all cases, the pulse period is 20 s.

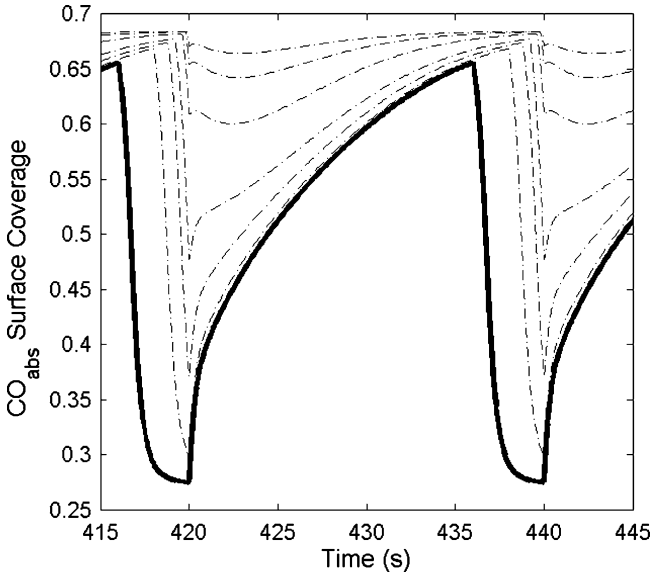

Fig. 12. Transient surface coverage θ_{CO}, at periodic steady state on the anode catalyst over one pulse cycle for duty ratios of 0.2 (solid line), 0.1, 0.06, 0.04, 0.02, 0.01 and 0.005. In all cases, the pulse period is 20 s.

the extremes, the largest incremental increases in potential occur near pulse duties of 2%. The lack of response at either extreme can be explained by the results in Fig. 12, which shows the effect of the duty ratio on the amount of CO_{ads} purged from the anode surface. In this case, the pulse duration must be sufficiently long before a significant amount of CO_{ads} can be oxidized. On the other hand, if an excessively long pulse is applied, no additional CO_{ads} can be removed.

A summary of how competing pulse regimes affect the average terminal voltage of the DMFC is given in Fig. 13, which plots the additional voltage above the amount that is normally generated by the fuel cell when loaded by an equivalent constant current (later analysis compares the performance of the DMFC based on equivalent power loads). The equivalent current loads are equal to the average of the pulse current calculated by (26) in Table 1 or from the duty ratio according to the following:

$$I_{load} = (1 - d)i_{low} + di_{high} \quad (44)$$

The plot shows cases for periods of 1.0, 2.5, 5.0 and 20 s, and in each case the potentials are averaged over the entire pulse cycle using (27) in Table 1. The maximum voltage gain is almost 40 mV and occurs within a period of about 2.5–5.0 s and an average pulse-current range of about 60–70 mA cm^{-2}. The average voltages decrease when the pulse periods are short because the oxidation period is not sufficient to decrease the amount of CO_{ads} on the anode surface. Alternatively, when the pulse period is long, the surface concentration of CO_{ads} is allowed to fully evolve between oxidation cycles, thereby limiting the effect of the pulse-loading routine.

Fig. 14 provides some insight into how pulsed loading affects the efficiency of the device. This plot shows the ratio of energy supplied to the load versus the total energy extracted from the methanol fuel as a function of time, such that the value at the end of the pulse cycle corresponds to the efficiency of the DMFC as defined in (25). As in the earlier case, the pulse cycle is 20 s. During the low-current duration of the pulse, the energy ratio of the device is improved by a peak factor of about 1.12 between the duties of 0.5% and 20%, and this improvement can be attributed to the decreased amount of CO_{ads} and to the higher average potential of the DMFC. When the current is stepped up, the fraction of power supplied to the load increases steeply for about 2 s, and the boost occurs because the fuel cell potential drops slowly as CO_{ads} is purged from the surface (note in Fig. 11 that the sluggish response is not repeated when the current is stepped back down). After the 2-s duration, the energy ratio continues to increase because the fuel cell has transitioned to a more efficient

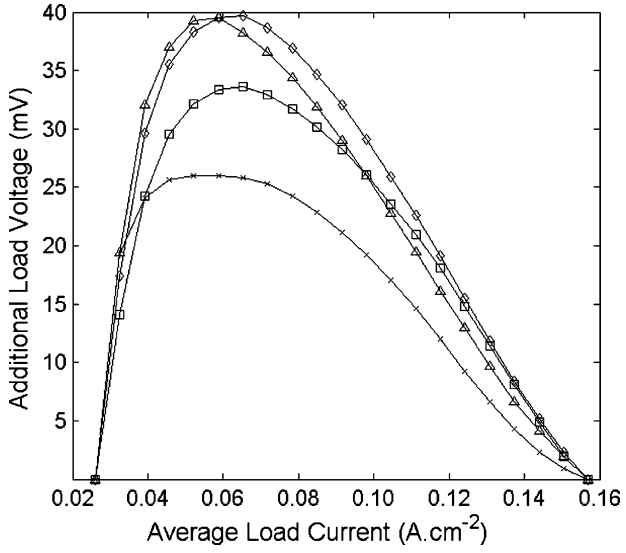

Fig. 13. Additional voltage (averaged over one pulse cycle) sourced to the load when the DMFC is pulsed-current loaded vs. when the fuel cell is loaded with an equivalent constant current. Pulse periods are 20 (×), 5.0 (△), 2.5 (◊) and 1.0 s (□).

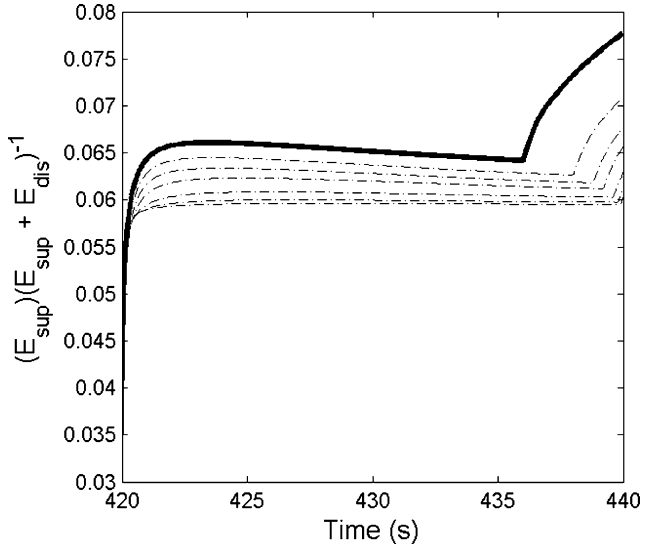

Fig. 14. Transient energy ratios (energy supplied to the load vs. the total energy consumed by the fuel cell) plotted over one pulse cycle at periodic steady state. Duty ratios are 0.2 (solid line), 0.1, 0.06, 0.04, 0.02, 0.01 and 0.005. In all cases, the pulse period is 20 s.

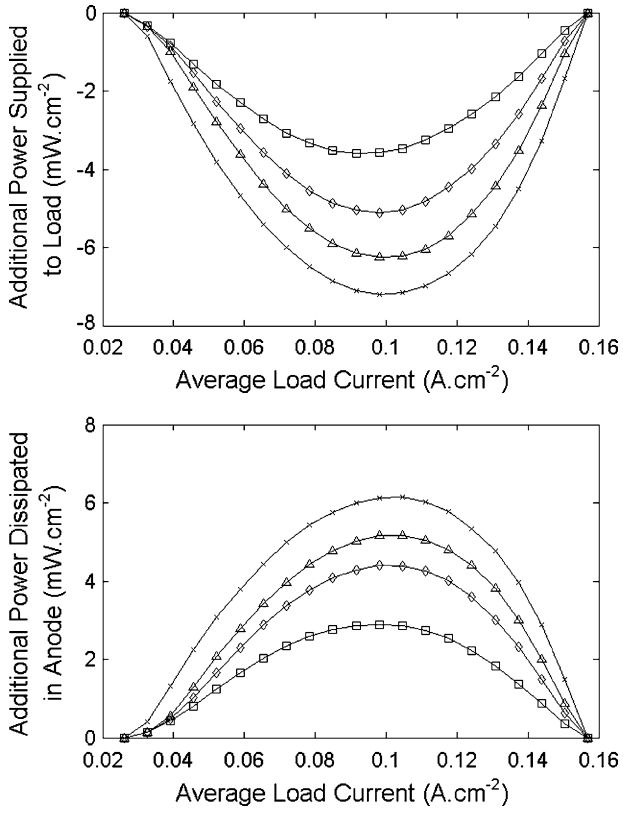

Fig. 15. Additional power transferred to the load when the fuel cell is pulsed vs. equivalently loaded with a constant current (top), and the respective amounts of power that are additionally dissipated in the anode (bottom). Pulse periods are 20 (×), 5.0 (△), 2.5 (◊) and 1.0 s (□).

operating point, 0.157 A cm^{-2}, and if the higher current were maintained for a long time, the energy ratio would eventually rise above 10% as it approached the steady-state value shown in Fig. 5.

Thus far, the simulation analysis has shown that pulsed loading improves the average potential of the DMFC and that it increases the energy transfer efficiency during the post-cleansing phase of the current pulse. However, further analysis indicates that pulse loading is not the superior operating method. In the top plot of Fig. 15, results comparing the pulsed-current and equivalent constant-current load methods show the difference in average power transferred to the load, and under every pulsed condition tested, the amount of average power transferred when the DMFC is pulsed is less than when it is loaded by an equivalent constant current. Moreover, as the pulse period is increased, less and less average power is transferred from the fuel cell. The bottom plot shows that when the fuel cell current is pulsed, most of the power not transferred to the load dissipates in the anode reaction as activation energy. The plot in Fig. 16 summarizes the results of this analysis, showing that the equivalent-current loading method is more efficient than pulse loading regardless of the power transferred to the load (average powers are calculated by (28) and (29) in Table 1). In other words, this additional analysis shows that pulse loading may negatively affect the efficiency of the DMFC, rather than improve it. This result is contrary to earlier experimental reports, but those reports only demonstrated that pulse loading improves the terminal potential of the DMFC, which we have shown does increase, even while the net efficiency decreases.

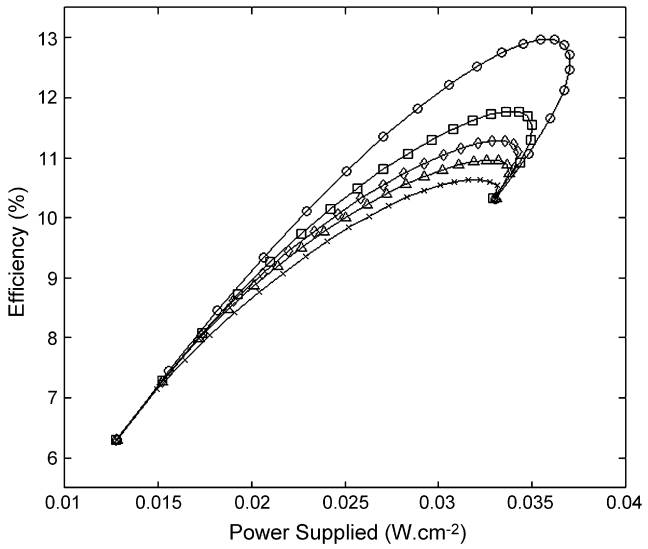

Fig. 16. Efficiency of the fuel cell as a function of the average power supplied to the load under a constant current (◯) and pulsed currents with periods of 20 (×), 5.0 (△), 2.5 (◊) and 1.0 s (□).

4. Conclusion

The method of intermittently cleansing adsorbed CO from a DMFC anode was analyzed using a transient domain model of the DMFC and the method was shown to be an ineffective way to increase the energy efficiency of the fuel cell. The analysis employed a new system level model that, unlike previous system-level models, retained states for three reaction intermediates on the catalyst surface so that the step response of the DMFC could be predicted over a full range of load currents, including steps down to no load and up to full load. Using model parameters identified from published experimental data, the transient dynamics of the system were modeled and analyzed. The voltage response following a step down to zero-current showed that the anode kinetics can account for nearly the entire overshoot of voltage above the normal open-circuit potential, and the magnitude of that overshoot appears to be related to the non-minimum phase response of the hydrogen adsorbate. Although intermittent pulses of increased current within the nominal operating range of the DMFC were shown to periodically cleanse the CO from the catalyst and thereby boost the average potential of the fuel cell, a more detailed analysis revealed that the pulsed-current approach actually dissipates more energy in the anode reaction than it produces, thus making it less efficient than operating at constant current.

References

[1] L. Carrette, K.A. Friedricj, M. Huber, U. Stimming, Phys. Chem. Chem. Phys 3 (2001) 320–325.
[2] J. Kallo, J. Kamara, W. Lehnert, R. Helmont, J. Power Sources 127 (2004) 181–186.

[3] P. Argyropoulos, K. Scott, W.M. Taama, J. Power Sources 87 (2000) 153–161.
[4] P. Argyropoulos, K. Scott, W.M. Taama, Electrochim. Acta 45 (2000) 1983–1998.
[5] J. Yoo, H. Choi, J. Nam, Y. Lee, C. Chung, E. Lee, J. Lee, S. Cho, J. Power Sources 158 (2006) 13–17.
[6] M. Neergat, T. Seiler, E.R. Savinova, U. Stimming, J. Electrochem. Soc. 153 (2006) 997–1003.
[7] Hamnett, Catal. Today 38 (1997) 445–457.
[8] J. Divisek, J. Fuhrmann, K. Gartner, R. Jung, J. Electrochem. Soc. 150 (2003) 811–825.
[9] P.S. Kauranen, E. Skou, J. Munk, J. Electroanal. Chem. 404 (1996) 1–13.
[10] M.R. Shivhare, R.G. Allen, K. Scott, A.J. Morris, E.B. Martin, J. Electroanal. Chem. 595 (2006) 145–151.
[11] T. Vidakovic, M. Christov, K. Sundmacher, J. Electroanal. Chem. 580 (2005) 105–121.
[12] K. Scott, P. Argyropoulos, J. Power Sources 137 (2004) 228–238.
[13] K. Sundmacher, T. Schultz, S. Zhou, K. Scott, M. Ginkel, E.D. Gilles, Chem. Eng. Sci. 56 (2001) 333–341.
[14] U. Krewer, K. Sundamacher, J. Power Sources 154 (2005) 153–170.
[15] T. Iwasita, Electrochim. Acta 47 (2002) 3663–3674.
[16] H. Dohle, J. Mergel, D. Stolten, J. Power Sources 111 (2002) 268–282.
[17] Z.H. Wang, C.Y. Wang, J. Electrochem. Soc. 150 (2003) 508–519.
[18] X. Ren, T.E. Springer, S. Gottesfeld, J. Electrochem. Soc. 147 (2000) 92–98.
[19] J. Nordlund, G. Lindbergh, J. Electrochem. Soc. 151 (2004) 1357–1362.
[20] M. Ceraolo, C. Miulli, A. Pozio, J. Power Sources 113 (2003) 131–144.
[21] F.N. Buchi, G.G. Scherer, J. Electrochem. Soc. 148 (2001) 183–188.